Journal of Applied Physics

Dielectric and conducting properties of unintentionally and Sn-doped β-Ga_2O_3 studied by terahertz spectroscopy

Cite as: J. Appl. Phys. **127**, 165702 (2020); https://doi.org/10.1063/1.5143735
Submitted: 23 January 2020 . Accepted: 11 April 2020 . Published Online: 29 April 2020

Nick Blumenschein, Christelle Kadlec, Oleksandr Romanyuk, Tania Paskova, John F. Muth, and Filip Kadlec

Journal of Applied Physics ARTICLE scitation.org/journal/jap

Dielectric and conducting properties of unintentionally and Sn-doped β-Ga_2O_3 studied by terahertz spectroscopy

Cite as: J. Appl. Phys. **127**, 165702 (2020); doi: 10.1063/1.5143735
Submitted: 23 January 2020 · Accepted: 11 April 2020 ·
Published Online: 29 April 2020

View Online Export Citation CrossMark

Nick Blumenschein,[1] Christelle Kadlec,[2] Oleksandr Romanyuk,[2] Tania Paskova,[1] John F. Muth,[1] and Filip Kadlec[2,a)]

AFFILIATIONS

[1]Department of Electrical and Computer Engineering, North Carolina State University, Raleigh, North Carolina 27695, USA
[2]Institute of Physics, Czech Academy of Sciences, Na Slovance 2, 182 21 Prague 8, Czech Republic

[a)]**Author to whom correspondence should be addressed:** kadlecf@fzu.cz

ABSTRACT

Dielectric and conducting properties of unintentionally doped bulk and Sn-doped thin film β-Ga_2O_3 samples were studied using time-domain terahertz spectroscopy. Complex permittivity and optical conductivity spectra from 0.25 to 2.5 THz were obtained experimentally over a broad temperature range. The low-temperature spectra of the unintentionally doped sample were fit using a model involving two oscillators. The parameters of one of them show an unusual temperature dependence, in particular, a pronounced increase in the oscillator strength upon heating above 50 K. This is interpreted as an absorption due to thermally activated charge carriers moving in localized potential minima linked to the unintentional doping. Upon heating, the influence of this optical conductivity mechanism strongly increases, and the sample becomes opaque in the THz range near 100 K. The nanocrystalline Sn-doped Ga_2O_3 thin film sample exhibits a much higher optical conductivity than the unintentionally doped bulk sample, and its spectra are remarkably stable over a broad temperature range (4–750 K). This first study of β-Ga_2O_3 based on phase-sensitive THz spectroscopy reveals how the impurities influence the high-frequency conductive properties of the material.

I. INTRODUCTION

Recently, gallium oxide has been studied extensively because of its excellent material properties. It features a wide bandgap of $E_g = 4.9$ eV, a critical electric field strength of $E_c = 8$ MV/cm, a maximum theoretical electron mobility of $\mu_e = 250\ \mathrm{cm^2/(V\,s)}$ between 300 and 500 K,[1] and a static relative permittivity of $\varepsilon = 10$. Baliga's figure of merit—the product $\varepsilon\mu_e E_c^3$ divided by the one for Si—is commonly used for describing the suitability of semiconductors in high-power device applications by considering how well the material conducts when subject to a particular breakdown voltage;[2] β-Ga_2O_3 attains a value of 2870, which is significantly higher than in other wide bandgap materials such as SiC (340) and GaN (870).[3] These properties make β-Ga_2O_3 successful in semiconductor devices such as solar-blind UV photodetectors,[4–6] Schottky barrier diodes,[7–9] and field-effect transistors.[10–12] The development of high-power devices has been an emphasis of research involving β-Ga_2O_3, but it is also a promising material for high-frequency applications.[13] Johnson's figure of merit,[14] which describes a material's capability for use in applications where high-frequency and high-power is of interest, once again shows an advantage of β-Ga_2O_3 (Johnson's figure of merit of 2844) over SiC (278) and GaN (1089).[15] Furthermore, recent developments in Ga_2O_3-based MOSFET processing have resulted in power gains greater than 10 dB for high-frequency switching speeds over 3 GHz.[16]

To ensure future success using Ga_2O_3 in the development of high-frequency devices, it is important that many of its material properties are studied up to the GHz/THz frequency regime. Although some recent studies[17,18] dealt with the DC and low-frequency AC dielectric properties, there is still a lack of information about the high-frequency AC properties of the crystals, both intentionally and unintentionally doped (UID); in the latter case, ppm concentrations of Al, Si, Cl, and 15 other elements are unavoidably present due to the growth technology.[19] Furthermore, because of the relatively low thermal conductivity of Ga_2O_3 when

compared to SiC and GaN,[20] it is also crucial to understand the effects of temperature in the high-frequency domain. THz time-domain spectroscopy (TDS) is the method of choice for characterizing materials under such conditions. THz TDS has been used to characterize a wide variety of semiconductor materials such as GaN,[21–23] graphene,[24–26] and conducting oxides like ZnO,[27,28] Na_xCoO_2,[29] and $BaSnO_3$.[30] To our knowledge, there is only one brief report using THz TDS for determining THz properties of β-Ga_2O_3 at room temperature[31] which is discussed in detail below. The present work is focused on experimental findings on the THz response of β-Ga_2O_3 for varying temperature conditions and doping.

II. SAMPLES AND EXPERIMENTAL DETAILS

Single-crystalline ($\bar{2}01$)-oriented β-Ga_2O_3 bulk samples were grown by Tamura Corporation using edge-defined film-fed growth[19] and polished to a uniform thickness of 650 μm. UID and Sn-doped bulk β-Ga_2O_3 samples had nominal room-temperature free carrier concentrations of 2.2×10^{17} cm^{-3} and 4.6×10^{18} cm^{-3}, respectively. The unit cell of β-Ga_2O_3 and the crystallographic scheme of the ($\bar{2}01$)-oriented sample are shown in Fig. 1.

A 1.15 μm thick ($\bar{2}01$)-oriented Sn-doped thin film was grown using pulsed laser deposition on a 430 μm thick c-plane sapphire substrate at 890 °C in a 13 mPa oxygen ambient. For the pulsed laser deposition, a 248 nm KrF excimer laser was used with a 10 Hz repetition rate and energy of ≈250 mJ/pulse. An ablation target containing 10 mol. % SnO_2 was formed by hydraulic pressing and sintering of 99.999%-pure gallium oxide and tin oxide powders at 1600 °C. Room-temperature Hall measurements were made on the sample, revealing electrical conductivity, carrier concentration, and mobility values of 0.029 $(\Omega\,\mathrm{cm})^{-1}$, 7.3×10^{16} cm^{-3}, and 2.5 cm^2 $(\mathrm{V\,s})^{-1}$. We verified that the in-plane THz response of the sample was isotropic, indicating a polycrystalline textured structure of the thin film.

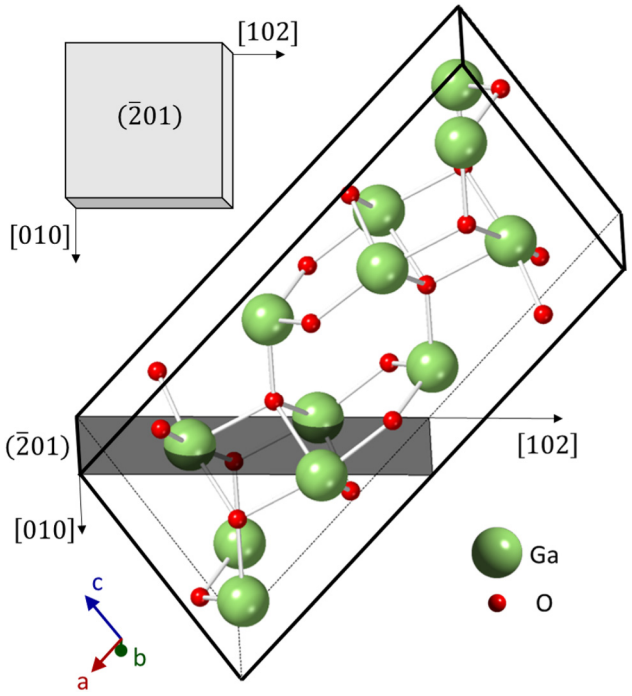

FIG. 1. Unit cell of β-Ga_2O_3 and orientation of the bulk samples cut along the ($\bar{2}01$) plane. Inset: schematic view of the sample showing the two orientations of the THz electric field E applied parallel with the [010] and [102] directions.

A custom-made setup was used for time-domain THz spectroscopy measurements. The laser oscillator source (Mira, Coherent) provided a beam with an 810 nm center wavelength, 80 fs pulse length, and a 76 MHz repetition rate. These laser pulses excited a biased large-area interdigitated photoconductive THz emitter, which radiated linearly polarized THz pulses that probed the samples. Pulses transmitted through the samples were detected by balanced photodiodes for electro-optic sampling based on the Pockels effect in a 1 mm-thick (110)-oriented ZnTe crystal. To avoid water vapor absorption, the whole THz beam path was enclosed in a vacuum chamber which was kept at a pressure of a few mbar during measurements. The samples were placed in a He-flow optical cryostat (Optistat, Oxford Instruments) with mylar windows, and its temperature was varied from 4 to 300 K. For the bulk UID sample, measurements at temperatures higher than 80 K were not feasible since the sample became opaque.

By taking the Fourier transform of the time-domain THz spectra, we obtained the frequency (f) dependent complex transmittance, which was then used to numerically calculate the complex refractive index spectra $N(f)$. These spectra can be equivalently converted to those of relative permittivity, $\varepsilon(f) = \varepsilon'(f) + \mathrm{i}\varepsilon''(f) = N^2(f)$, or to optical conductivity spectra, $\sigma(f) = \sigma'(f) + \mathrm{i}\sigma''(f)$, which are linked by the relation $\sigma(f) = 2\pi i f \varepsilon_0 \varepsilon(f)$, where ε_0 denotes the vacuum permittivity. More details on data treatment and examples of obtained data can be found in the supplementary material.

Complex THz transmittance of the thin film sample was measured at low temperatures in the cryostat and above room temperature. To this aim, we employed an adapted commercial high-temperature cell (Specac) installed in the vacuum chamber. The cell was equipped with a custom-made sample positioning device designed to improve the measurement reliability. This was achieved by collecting consecutively the time-domain waveforms of both the film on the substrate and a reference sapphire substrate with the same thickness for each temperature. More experimental details and the way of obtaining the $N(f)$ spectra of films can be found in Ref. 32.

III. RESULTS AND DISCUSSION

A. Bulk samples

For spectroscopic measurements of the UID sample, we applied the E-vector parallel with the edges of the sample, which were aligned with the [010] and [102] crystallographic directions. We note that in monoclinic crystals, the permittivity is a tensor whose axes depend on the wavelength if absorption is present. Moreover, the axes for the real and imaginary parts of the permittivity tensor may not coincide.[33] Consequently, birefringence occurs in β-Ga_2O_3, inducing a mixed polarization of linearly

polarized incident and outgoing beams. For this reason, it is not easy to rigorously evaluate the components of the permittivity tensor. These anisotropic properties originate in the contribution of the crystal lattice, i.e., in the phonon modes. However, as we show below, our work is focused on an additional contribution which is not related to phonons. Within the precision of our measurements, the response of this contribution appears to be isotropic, so studying either of the two polarizations is sufficient for the present purpose.

Although all the complex spectra of optical constants—$N(f)$, $\varepsilon(f)$, and $\sigma(f)$—are mathematically equivalent, a choice can be made for treating the results. Whereas, for dielectrics, the permittivity spectra $\varepsilon(f)$ are often used, in semiconducting and conducting systems, it is quite common to draw the conductivity spectra $\sigma(f)$. In the case of resonances exhibiting a behavior of damped harmonic oscillators, the spectra of the real part of the conductivity $\sigma'(f) = -\varepsilon''(f)\,2\pi f\varepsilon_0$ have the advantage of showing peaks exactly at the oscillation frequencies; in contrast, the peaks in $\varepsilon''(f)$ are influenced by the damping. Therefore, we deem it most convenient to use the real part of permittivity $\varepsilon'(f)$ and the real optical conductivity $\sigma'(f)$ spectra for both drawing and modeling the material response. Figure 2 shows these spectra of the UID sample, measured with electric field E aligned with the [102] direction at various temperatures and for comparison, those taken at two temperatures with $E \parallel [010]$. The spectra of the imaginary part of permittivity $\varepsilon''(f)$ are shown in Fig. S3 in the supplementary material.

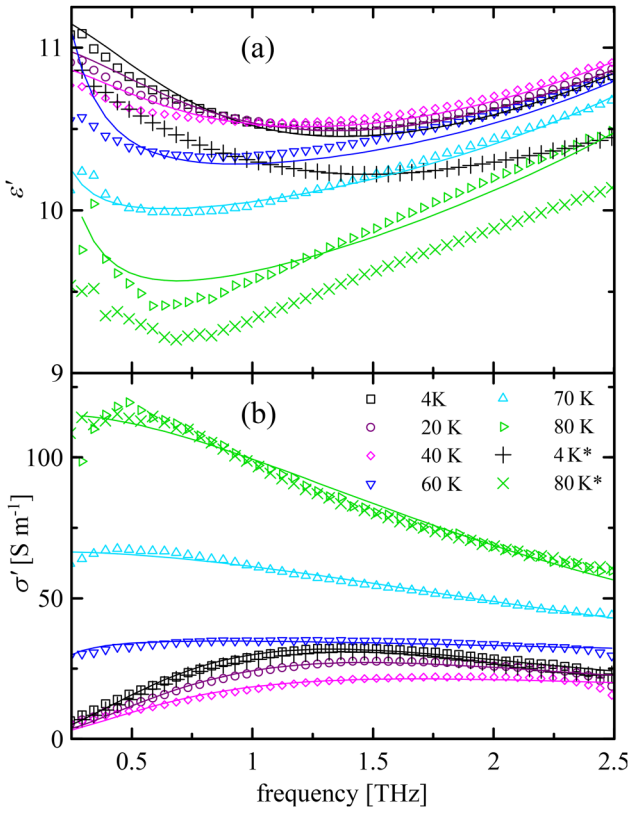

FIG. 2. Real permittivity (a) and optical conductivity (b) spectra of UID bulk β-Ga_2O_3 with $E \parallel [102]$ (open symbols) obtained by THz TDS and the corresponding fits (lines) using Eq. (1). For comparison, two spectra obtained in the $E \parallel [010]$ geometry are shown by crosses and marked by asterisks in the key.

The values of all permittivity spectra are close to ten, whereas the optical conductivity values vary between tens and 100 $(\Omega\,\mathrm{m})^{-1}$. For $E \parallel [010]$, the permittivity values are systematically lower (by $\approx$0.25) than those of the spectra for $E \parallel [102]$. In contrast, the optical conductivity spectra for both orientations are indistinguishable within the experimental error of $\approx \pm 5\,(\Omega\,\mathrm{m})^{-1}$. For both orientations, the same temperature evolutions were observed (see Fig. S2 in the supplementary material). Thus, the measured anisotropy of the THz spectra is very weak, which is in agreement with recent room-temperature infrared ellipsometric measurements and numerical simulations of permittivity tensors spectra in different directions, performed for frequencies above 4 THz;[34] for the different directions, the reported room-temperature permittivity spectra extrapolate to very similar values in the THz range.

As stated above, our experimental data reveal low anisotropy at THz frequencies for the studied temperature range. This anisotropy is, due to phonons, the oscillation frequencies of which are located at frequencies of $\approx$6.5 THz or above.[34] As we will show below, in the THz range we studied, the phonons provide only a smooth background profile that adds up with the observed dispersion, whose origin is different from phonons. Since our results show that the additional dispersion is isotropic (within the sample plane and in the limits of our experimental accuracy; see Fig. 2), and because the THz spectra of β-Ga_2O_3 yield no useful information on phonons, it is sufficient to study one of the orientations of the sample. The conclusions then apply equally to all directions of the incident THz field within the sample plane.

As one can see from Fig. 2, the temperature dependence of the THz spectra is not monotonic. In fact, the spectral evolution is different in two distinct temperature intervals with a transition around 40 K. Below this value, a slight increase in $\varepsilon'(f)$ with T above $\approx$1 THz and a slow decrease at sub-THz frequencies are observed, whereas the THz optical conductivity spectra exhibit a gradual decrease over the whole spectral range. In contrast, above 40 K, the spectra of $\varepsilon'(f)$ drop somewhat faster with temperature at all frequencies, and the optical conductivity spectra $\sigma'(f)$ rise sharply with temperature; also their shape changes, as a pronounced increase in $\sigma'(f)$ toward low f turns up.

In order to describe the spectra, we fitted the experimental data for $E \parallel [102]$ using different models of the complex permittivity. It is quite obvious that the standard Drude model is not able to describe the spectra, because it predicts a spectral shape distinctly different from our observations. This is shown in detail in Fig. 3 for the pair of $\varepsilon'(f)$, $\sigma'(f)$ spectra obtained at 70 K. In the experimentally obtained data, a distinct increase in the $\varepsilon'(f)$ values toward low frequencies is observed at all temperatures. In contrast, the Drude model always provides the opposite trend. Furthermore, it predicts $\sigma'(f)$ spectra which drop monotonically with frequency, whereas we clearly observe local maxima in $\sigma'(f)$. These maxima in $\sigma'(f)$ could be, in principle, reproduced by the Drude–Smith model,[35] which introduces an additional parameter $-1 \le c \le 0$

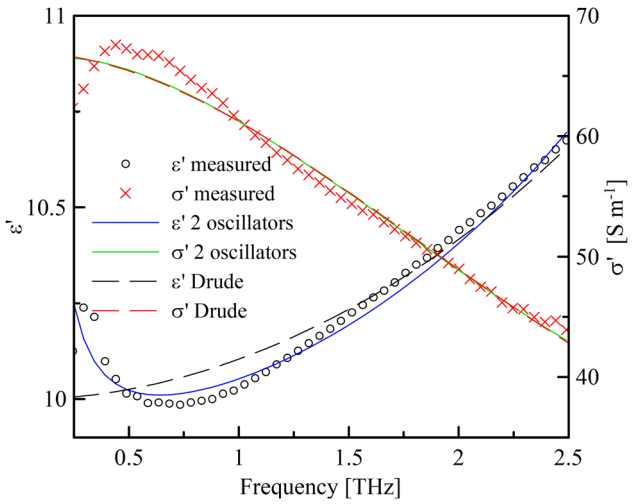

FIG. 3. Spectra of UID β-Ga_2O_3 obtained experimentally at $T = 70$ K (symbols) and their fits (lines) based on different models of the complex permittivity. The best match is observed for a model with two oscillators [Eq. (1)], which is the only one providing simultaneously the observed decrease in $\sigma'(f)$ and increase in $\varepsilon'(f)$ toward low frequencies.

describing the so-called "persistence of velocity." This concept, without an *a priori* clear microscopic interpretation,[36] is able to describe mathematically the spectra of some conductive materials, where the classical Drude model fails. In an extreme case, where $c = -1$, the DC conductivity is suppressed, which implies a charge confinement. When modeling the spectra shown in Fig. 3, we found, however, that even the Drude–Smith model converged to the value of $c = 0$, yielding no improvement with respect to the Drude model. Thus, we find these models unsuitable for the UID β-Ga_2O_3 bulk sample, as they do not predict the observed increase in ε' at low frequencies.

Here, we would like to discuss briefly the results of THz reflectance published earlier by Saito *et al.*[31] The aim of their paper was to estimate the free carrier concentrations in various β-Ga_2O_3 samples from the reflectance spectra. It is important to note that the work only studied the amplitude reflectance without any phase sensitivity. Consequently, that work is very different from our results based on complex transmittance measurements, because the fits by the Drude model reported in Ref. 31 are merely based on a hypothesis of the Drude model suitability. This hypothesis could not be confirmed because the reflectance phase was not determined.

In the present case, as illustrated in Fig. 3, the best match with our experimental results was found using a model involving two harmonic oscillators, which appears to be also the simplest one providing a satisfactory data description. It is given by the formula

$$\varepsilon(f) = \varepsilon_\infty + \sum_{i=1,2} \frac{\Delta\varepsilon_i f_i^2}{f_i^2 - f^2 - \mathrm{i}\gamma_i f}, \tag{1}$$

where ε_∞ denotes the sum of dielectric strengths of the high-frequency phonons; f_i, $\Delta\varepsilon_i$, and γ_i mark the oscillation frequencies, dielectric strengths, and damping constants of the oscillators, respectively. For the fitting procedure, the spectra of the imaginary part of permittivity $\varepsilon''(f)$ were converted to the real part optical conductivity $\sigma'(f)$ in order to provide a better insight into the AC transport mechanisms.

The terms used in Eq. (1) appear to be the most convenient for effectively modeling the experimental data. The first oscillator [$i = 1$ in Eq. (1)] is at the origin of the observed permittivity increase toward lower frequencies, and the other ($i = 2$) corresponds to a phonon located beyond the accessible spectral range. Phonons in β-Ga_2O_3 were recently studied[34] at room temperature, experimentally and theoretically. For the purpose of modeling the present spectra, where only the low-frequency tail of the lowest-lying phonons plays a role, we used one harmonic oscillator with adequate parameters providing a good agreement both with the measured spectra and with the parameters reported in Ref. 34 (listed in Table II for the B_u-symmetry mode with $k = 8$). The parameters used in our fit were as follows: $f_2 = 6.5$ THz, $\Delta\varepsilon_2 = 3$, and $\gamma_2(T) = (0.03 + T \times 10^{-4}/\mathrm{K})$ THz. This temperature dependence of the damping is a linear interpolation between the room-temperature value from Ref. 34 and the one estimated at $T = 0$ K, $\gamma_2(0) = 0.03$ THz $= 1\,\mathrm{cm}^{-1}$. For ε_∞, the fits yielded almost temperature-independent values of 7.3 ± 0.1. Note that this value includes the total contribution of phonons except the dielectric strength of the one described by the second oscillator. Thus, it cannot be directly compared with the values of ε_∞ usually obtained by infrared spectra fitting, which are defined differently.

In Fig. 2, the solid lines show the spectra of permittivity and optical conductivity calculated using the optimized parameters. Overall, the fits describe the experimental spectra very well. A moderate mismatch in the real part of conductivity spectra is observed below 0.5 THz; it appears at 60 K and it weakly increases with temperature. We attribute this mismatch to an anharmonicity of the underlying potential, whereas Eq. (1) assumes a parabolic one. As we show below, this temperature range corresponds to a transition from one oscillatory regime to another one, which is a situation where the anharmonicity is likely.

The optimized parameters of the first oscillator obtained from spectra fitting at all temperatures are shown in Fig. 4. This oscillator exhibits a very unusual temperature dependence. At the lowest temperature ($T = 4$ K), its oscillation frequency amounts to $f_1 \approx 1.3$ THz, which manifests itself clearly by a broad maximum in the optical conductivity spectra [see Fig. 2(b)]. Upon heating, f_1 slowly rises, reaching 1.5 THz at 50 K; this is followed by its sudden drop down to ≈0.2 THz at 80 K. The transition between the trends, near 50–60 K, can be equally observed in the other parameters. The damping constant γ_1 reaches a maximum of ≈6 THz at 60 K. Also, the dielectric strength $\Delta\varepsilon_1$ deduced from the fits displays an anomaly: we observed its mild decrease for temperatures up to 40 K, and above 50 K, a dramatic increase by up to two orders of magnitude [see Fig. 4(b)]. At $T = 80\,K$, we observed a value of $\Delta\varepsilon_1 \approx 80$.

In the whole temperature range, the damping constant γ_1 is much higher than the oscillation frequency f_1; thus, this oscillator is overdamped. These oscillator parameters are very different from

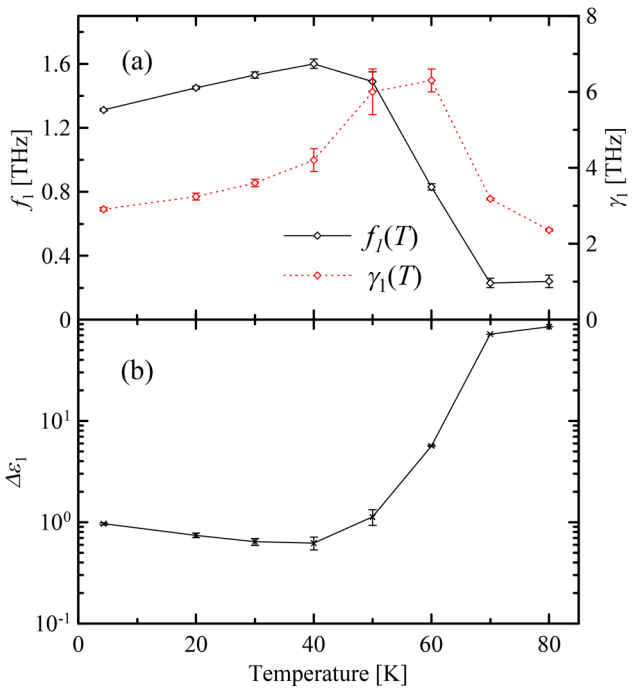

FIG. 4. Temperature dependences of fit parameters used in Eq. (1) to describe the $\varepsilon'(f)$, $\sigma'(f)$ spectra shown in Fig. 2: (a) eigenfrequency f_1, oscillator damping γ_1, and (b) dielectric strength $\Delta\varepsilon_1$. Wherever the error bars are not seen, their extent is smaller than the symbol size. The lines are guides for the eye only.

those usually observed for phonons; this holds true, in particular, for the strong increase in the dielectric strength with temperature occurring near 60 K. Given the fact that it is the oscillator model which describes the spectra well, the charge carriers are localized, and their presence is likely due to the unintentional doping. In other words, the atoms coming from the unintentional doping are fixed within the Ga_2O_3 lattice, and they are accompanied by additional charge carriers which remain close to these impurities.

Such a behavior is not common in semiconductors; we attribute their origin to the known fact that a broad variety of unintentional impurities are present in bulk β-Ga_2O_3 crystals grown by edge-defined film-fed growth.[19] It is thought that these impurities give rise to a complex crystal potential for the uncompensated charges, featuring various energy barriers. Then, the observed temperature evolution can be explained by a combination of two oscillatory regimes, one of which is dominant at temperatures below 50 K and the other for $T > 60$ K; this temperature corresponds to an activation energy of about 5 meV, which is likely linked to some unintentional dopants. For $T < 50$ K, the charges exhibit an oscillation frequency between 1.3 and 1.5 THz, and their contribution to the permittivity is quite weak, $\Delta\varepsilon < 1$. In contrast, for $T > 60$ K, we observed a substantially lower oscillation frequency, near 0.2 THz, and their contribution to the relative permittivity attains up to 80. This may be due to a higher number of (thermally activated) charge carriers involved for $T > 60$ K, their greater delocalization, or both. Finally, let us note that Víllora *et al.*[37] have reported anomalies in electrical conductivity and lattice parameters of floating-zone grown β-Ga_2O_3 single crystals, occurring at temperatures near 50 K. The origin of these anomalies remains unclear, since different sample growth methods were used in the study reported in Ref. 37 and ours. In both cases, Si impurities are reported, but the link between this anomaly and the impurities cannot be confirmed at this time.

Although the results obtained by THz spectroscopy do not allow for establishing a more detailed microscopic picture, we can conclude that these localized charge carriers might play an important role in potential components for high-frequency electronics. In fact, our fits reveal a trend which can be extrapolated to higher temperatures, suggesting that the optical conductivity of the UID sample would amount to at least hundreds of $(\Omega\,\mathrm{m})^{-1}$ in the GHz range at room temperature [see Fig. 2(b)]. In order to avoid this GHz- and THz-range localized conductivity, one could consider introducing other dopants for charge compensation, similarly to the approach that has been reported for GaN.[21]

We also attempted to measure the Sn-doped bulk sample using THz TDS. However, it appeared that the sample was substantially more opaque than the UID one, and we were only able to detect a very weak transmitted waveform at $T = 4$ K, enabling us to evaluate the spectrum at frequencies below 0.75 THz. The spectrum for $E \parallel [010]$ is shown in Fig. 5; the optical conductivity is about one order of magnitude higher than in the case of the UID sample. At temperatures above 4 K, the sample was completely opaque, which precluded other THz TDS measurements. Based on an analogy to the UID sample, one can expect values of the room-temperature optical conductivity for doped bulk samples to be even higher than that of the UID sample. Given the sample opacity, it is not possible to make even a gross estimate of the room-temperature optical conductivity from our results. Nevertheless, it seems very likely that both unintentional and intentional doping will have a strong effect on the high-frequency electrical conductivity, unless the crystal is properly compensated.

B. Sn-doped thin film

Because of the high optical density of Sn-doped β-Ga_2O_3, we decided to study the THz transmittance of the material in the form of a thin film. The THz TDS measurements of the in-plane response were first performed at low temperatures ($T < 300$ K) and then in the high-temperature cell ($T > 300$ K). After the heating cycle, there was no visible sample degradation, and the room-temperature spectra were identical with those before heating.

We determined the complex refractive index spectra from the complex THz transmittance using the formula given in Ref. 32. From the refractive index spectra, we calculated those of $\varepsilon'(f)$ and $\sigma'(f)$ [see Fig. 5; the $\varepsilon''(f)$ spectra are shown in the Fig. S4 in the supplementary material]. Compared to the UID sample, these spectra of the Sn-doped thin film exhibit much higher values—the relative permittivity reaches several tens, and the optical conductivity is of the order of several thousand $(\Omega\,\mathrm{m})^{-1}$. Between 4 and 50 K, the same trend of decreasing permittivity upon heating as in

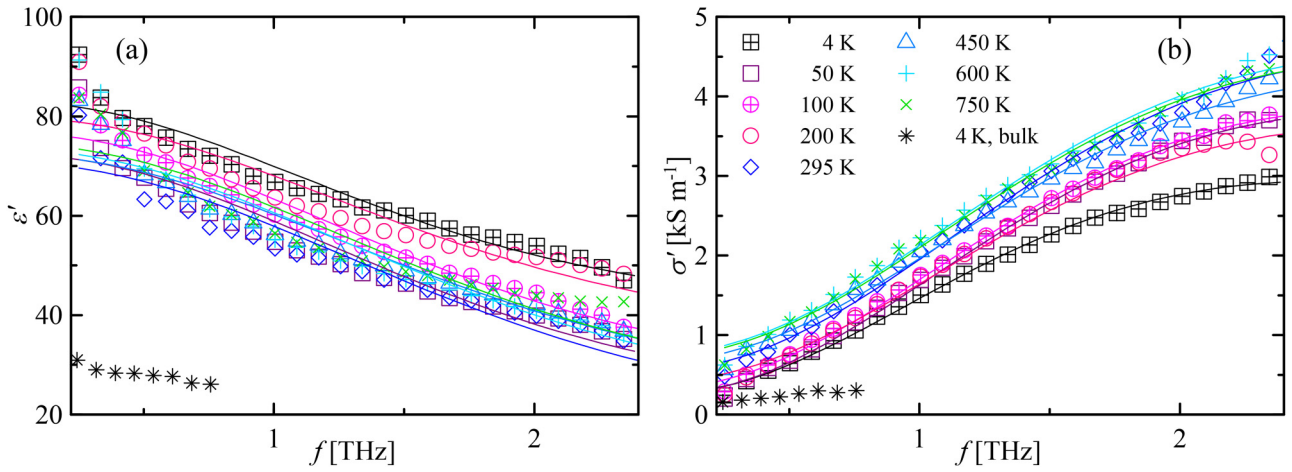

FIG. 5. Temperature dependence of the permittivity (a) and optical conductivity (b) spectra of Sn-doped β-Ga_2O_3 bulk sample ($E \parallel [010]$, $T = 4$ K; asterisks) and thin film (isotropic in-plane response; other symbols) measured by THz TDS. The lines represent fits using the Drude–Smith model;[35] the resulting parameters are plotted in Fig. 6.

the case of bulk β-Ga_2O_3 is observed, followed by a slight increase with T upon further heating.

The shapes of the spectra are quite different from those of the UID sample; $\varepsilon'(f)$ markedly drops with frequency, whereas $\sigma'(f)$ exhibits an approximately linear increase with frequency. As one can see from Fig. 5, there is also a substantial difference between the Sn-doped thin film and bulk spectra for $T = 4$ K. This is likely due to the different material growth technology used, as the bulk and thin film samples will have different crystalline and morphological properties. For the thin film, atomic force microscopy was used to obtain RMS roughness and average grain size values of ≈2 nm and 10 nm, respectively, which are consistent with previous reports on heteroepitaxial β-Ga_2O_3 grown on c-plane sapphire using pulsed laser deposition.[38,39] These measurements indicate that the thin film surface is quite smooth, yet the bulk β-Ga_2O_3 crystals still possess superior quality. The Sn-doped bulk crystal was found to have an RMS roughness of ≈0.6 nm and was absent of grains.

The only simple model able to adequately describe the thin film spectra appears to be one containing a Drude–Smith term[35] and a harmonic oscillator corresponding to the lowest-lying optical phonon,

$$\varepsilon(f) = \varepsilon_\infty - \frac{N_c \frac{e_0^2}{m_e}\tau}{(1-2\pi i f\tau)}\left[1+\frac{c}{(1-2\pi i f\tau)}\right]\frac{1}{2\pi f i\varepsilon_0} + \frac{\Delta\varepsilon_2 f_2^2}{f_2^2 - f^2 - i\gamma_2 f}, \tag{2}$$

where N_c denotes the charge carrier concentration, m_e and τ are their effective mass and scattering time, respectively, c denotes the Smith's backscattering coefficient, and ε_0 is the vacuum permittivity. The resulting spectra are shown by lines in Fig. 5. Although the model describes the real permittivity spectra $\varepsilon(f)$ with small deviations, there is an overall good agreement between the model and the experimental data. The temperature dependences of the fit parameters are plotted in Fig. 6.

The backscattering coefficient is close to $c = -1$, and with increasing temperature, its absolute value exhibits a weak decrease. Within the model, this can be interpreted as a slight drop in the probability of the charge carriers to be reflected on the grain boundaries. The temperature changes in the carrier concentration N_c and the scattering time τ are quite weak, so we are cautious about drawing conclusions from these dependences. We would also like to note that due to the shape of the spectra, there is a correlation (close to 1) between the parameters N_c and τ in the fitting procedure. Therefore, their values provided by the model may not be quite reliable. The fitting results can, however, serve as an indirect confirmation of the presence of nanoscopic grains in the thin film. It is worth noting that the charge carrier concentration obtained from the Drude term is very close to the nominal room-temperature value of that for the Sn-doped bulk sample, 4.6×10^{18} cm^{-3}. By contrast, for the thin film, the carrier concentration obtained from Hall measurements is ≈80 times lower. This is consistent with the hypothesis that the film exhibits a grain structure which limits the DC conductivity, whereas inside the grains, the properties of Sn-doped β-Ga_2O_3 are similar to those of the bulk crystal.

Interestingly, the THz spectra of the Sn-doped thin film are not very sensitive to temperature compared with the bulk sample. At low temperatures, whereas the optical constants of the bulk β-Ga_2O_3 change by orders of magnitude with heating, for the thin film, at any frequency, both $\varepsilon'(f)$ and $\sigma'(f)$ spectra vary at most by a few tens of percent between 4 K and room temperature. Likewise, between room temperature and 750 K, the spectral changes in the permittivity of the thin film are less than 10 % and its optical conductivity varies by at most 20 %. These observations are probably linked to the granular character of the sample; we conjecture that its conducting properties

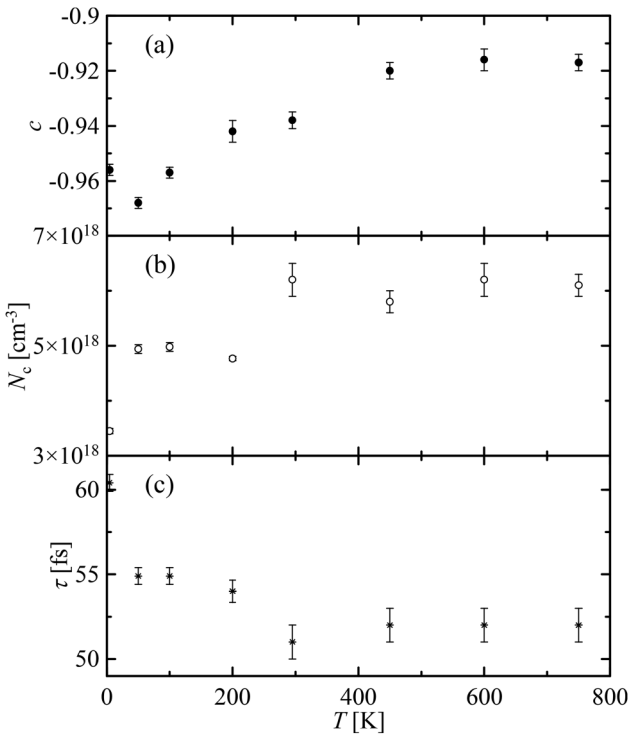

FIG. 6. Temperature dependences of the parameters describing the charge dynamics in the Sn-doped β-Ga_2O_3 thin film by the Drude–Smith model:[35] (a) backscattering coefficient c, (b) carrier concentration N_c, and (c) momentum scattering time τ. These values were obtained by fitting the THz spectra shown in Fig. 5 by Eq. (2).

are mainly determined by the confinement of charge carriers or by the conductivity of the grain boundaries. The observed low temperature variations of the high-frequency properties of the Sn-doped β-Ga_2O_3 thin films produced by pulsed laser deposition could, thus, be useful for electronics applications involving extreme temperature conditions or in cases where heating of the material by high current densities could occur.

IV. CONCLUSION

In conclusion, we have presented the first study on UID and Sn-doped β-Ga_2O_3 single crystals and a Sn-doped β-Ga_2O_3 thin film using phase-sensitive THz TDS over a wide temperature range. THz spectra of the UID sample are dominated by a harmonic oscillator term, whose strength dramatically increases for temperatures greater than 50 K. This reveals an oscillatory motion of localized charge carriers exhibiting two distinct regimes and involving an activation energy of ≈5 meV. Due to the opacity of Sn-doped crystals, a Sn-doped thin film was measured in a broad temperature range. The optical conductivity spectra of the thin film exhibit shapes which can be described using the Drude–Smith model. This is in agreement with the known presence of nanoscopic grains, which most probably determine the observed dynamics of localized charge carriers. In sharp contrast to the UID sample, the THz spectra of the Sn-doped film exhibited relatively low variations over a broad temperature range. In the future, we plan to expand on these findings by investigating β-Ga_2O_3 at sub-THz frequencies to gain additional insight into its AC dielectric properties and the underlying physical mechanisms.

SUPPLEMENTARY MATERIAL

In the supplementary material, we present additional details on data treatment in THz time-domain spectroscopy, including raw time-domain waveforms and their Fourier transforms. Furthermore, we show the temperature dependences of permittivity values for the two sample orientations studied and temperature-dependent imaginary permittivity spectra $\varepsilon''(f)$. Finally, we briefly introduce the atomic force microscopy measurements and reproduce the obtained topographical images.

ACKNOWLEDGMENTS

This work was supported by the Operational Program Research, Development, and Education financed by European Structural and Investment Funds, the Czech Ministry of Education, Youth, and Sports (Project No. SOLID21–CZ.02.1.01/0.0/0.0/16_019/0000760), and National Science Foundation (NSF) (Grant Nos. DMR-1506159 and OISE-1458427). C.K. also acknowledges the financial support from the Czech Science Foundation (Project No. 17-03662S).

REFERENCES

[1]N. Ma, N. Tanen, A. Verma, Z. Guo, T. Luo, H. G. Xing, and D. Jena, Appl. Phys. Lett. **109**, 212101 (2016).
[2]A. J. Green, K. D. Chabak, E. R. Heller, R. C. Fitch, M. Baldini, A. Fiedler, K. Irmscher, G. Wagner, Z. Galazka, S. E. Tetlak, A. Crespo, K. Leedy, and G. H. Jessen, IEEE Electron. Dev. Lett. **37**, 902 (2016).
[3]K. D. Chabak, K. D. Leedy, A. J. Green, S. Mou, A. T. Neal, T. Asel, E. R. Heller, N. S. Hendricks, K. Liddy, A. Crespo, N. C. Miller, M. T. Lindquist, N. A. Moser, R. C. Fitch, D. E. Walker, D. L. Dorsey, and G. H. Jessen, Semicond. Sci. Technol. **35**, 013002 (2019).
[4]L.-X. Qian, H.-F. Zhang, P. T. Lai, Z.-H. Wu, and X.-Z. Liu, Opt. Mater. Express **7**, 3643 (2017).
[5]F.-P. Yu, S.-L. Ou, and D.-S. Wuu, Opt. Mater. Express **5**, 1240 (2015).
[6]D. Guo, Z. Wu, P. Li, Y. An, H. Liu, X. Guo, H. Yan, G. Wang, C. Sun, L. Li, and W. Tang, Opt. Mater. Express **4**, 1067 (2014).
[7]M. Higashiwaki, K. Sasaki, H. Murakami, Y. Kumagai, A. Koukitu, A. Kuramata, T. Masui, and S. Yamakoshi, Semicond. Sci. Technol. **31**, 034001 (2016).
[8]Q. He, W. Mu, H. Dong, S. Long, Z. Jia, H. Lv, Q. Liu, M. Tang, X. Tao, and M. Liu, Appl. Phys. Lett. **110**, 093503 (2017).
[9]K. Konishi, K. Goto, H. Murakami, Y. Kumagai, A. Kuramata, S. Yamakoshi, and M. Higashiwaki, Appl. Phys. Lett. **110**, 103506 (2017).
[10]S. Krishnamoorthy, Z. Xia, C. Joishi, Y. Zhang, J. McGlone, J. Johnson, M. Brenner, A. R. Arehart, J. Hwang, S. Lodha, and S. Rajan, Appl. Phys. Lett. **111**, 023502 (2017).
[11]K. D. Chabak, N. Moser, A. J. Green, D. E. Walker, S. E. Tetlak, E. Heller, A. Crespo, R. Fitch, J. P. McCandless, K. Leedy, M. Baldini, G. Wagner, Z. Galazka, X. Li, and G. Jessen, Appl. Phys. Lett. **109**, 213501 (2016).
[12]M. J. Tadjer, N. A. Mahadik, V. D. Wheeler, E. R. Glaser, L. Ruppalt, A. D. Koehler, K. D. Hobart, C. R. Eddy, and F. J. Kub, ECS J. Solid State Sci. Technol. **5**, P468 (2016).
[13]M. Higashiwaki and G. H. Jessen, Appl. Phys. Lett. **112**, 060401 (2018).

[14]E. Johnson, RCA Rev. **26**, 163 (1965).
[15]S. J. Pearton, J. Yang, P. H. Cary, F. Ren, J. Kim, M. J. Tadjer, and M. A. Mastro, Appl. Phys. Rev. **5**, 011301 (2018).
[16]G. Jessen, K. Chabak, A. Green, J. McCandless, S. Tetlak, K. Leedy, R. Fitch, S. Mou, E. Heller, S. Badescu, A. Crespo, and N. Moser, in *2017 75th Annual Device Research Conference (DRC)* (IEEE, 2017), pp. 1–2.
[17]A. T. Neal, S. Mou, R. Lopez, J. V. Li, D. B. Thomson, K. D. Chabak, and G. H. Jessen, Sci. Rep. **7**, 13218 (2017).
[18]D. C. Look and K. D. Leedy, Sci. Rep. **9**, 1290 (2019).
[19]A. Kuramata, K. Koshi, S. Watanabe, Y. Yamaoka, T. Masui, and S. Yamakoshi, Jpn. J. Appl. Phys. **55**, 1202A2 (2016).
[20]M. Slomski, N. Blumenschein, P. P. Paskov, J. F. Muth, and T. Paskova, J. Appl. Phys. **121**, 235104 (2017).
[21]F. Kadlec, C. Kadlec, T. Paskova, and K. Evans, J. Phys. D Appl. Phys. **43**, 145401 (2010).
[22]W. Zhang, A. K. Azad, and D. Grischkowsky, Appl. Phys. Lett. **82**, 2841 (2003).
[23]T.-R. Tsai, S.-J. Chen, C.-F. Chang, S.-H. Hsu, T.-Y. Lin, and C.-C. Chi, Opt. Express **14**, 4898 (2006).
[24]P. R. Whelan, K. Iwaszczuk, R. Wang, S. Hofmann, P. Bøggild, and P. U. Jepsen, Opt. Express **25**, 2725 (2017).
[25]I. Ivanov, M. Bonn, Z. Mics, and D. Turchinovich, Europhys. Lett. **111**, 67001 (2015).
[26]X. Feng, M. Hu, J. Zhou, and S. Liu, J. Infrared Millim. Terahertz Waves **38**, 874 (2017).
[27]H. Němec, J. Rochford, O. Taratula, E. Galoppini, P. Kužel, T. Polívka, A. Yartsev, and V. Sundström, Phys. Rev. Lett. **104**, 197401 (2010).
[28]S. Bamini, H. Němec, K. Žídek, M. Abdellah, M. J. Al-Marri, P. Chábera, C. Ponseca, K. Zheng, and T. Pullerits, Phys. Chem. Chem. Phys. **19**, 6006 (2017).
[29]H. Němec, K. Knížek, Z. Jirák, J. Hejtmánek, M. Soroka, and J. Buršík, J. Phys. Condens. Matter **28**, 355601 (2016).
[30]S. Arezoomandan, A. Prakash, A. Chanana, J. Yue, J. Mao, S. Blair, A. Nahata, B. Jalan, and B. Sensale-Rodriguez, Sci. Rep. **8**, 3577 (2018).
[31]S. Saito, T. Onuma, K. Sasaki, A. Kuramata, N. Sekine, A. Kasamatsu, and M. Higashiwaki, in *2015 40th International Conference on Infrared, Millimeter, and Terahertz waves (IRMMW-THz)* (IEEE, 2015).
[32]F. Kadlec, C. Kadlec, P. Kužel, and J. Petzelt, Phys. Rev. B **84**, 205209 (2011).
[33]C. Sturm, R. Schmidt-Grund, C. Kranert, J. Furthmüller, F. Bechstedt, and M. Grundmann, Phys. Rev. B **94**, 035148 (2016).
[34]M. Schubert, R. Korlacki, S. Knight, T. Hofmann, S. Schöche, V. Darakchieva, E. Janzén, B. Monemar, D. Gogova, Q.-T. Thieu, R. Togashi, H. Murakami, Y. Kumagai, K. Goto, A. Kuramata, S. Yamakoshi, and M. Higashiwaki, Phys. Rev. B **93**, 125209 (2016).
[35]N. V. Smith, Phys. Rev. B **64**, 155106 (2001).
[36]T. L. Cocker, D. Baillie, M. Buruma, L. V. Titova, R. D. Sydora, F. Marsiglio, and F. A. Hegmann, Phys. Rev. B **96**, 205439 (2017).
[37]E. G. Víllora, K. Shimamura, T. Ujiie, and K. Aoki, Appl. Phys. Lett. **92**, 202118 (2008).
[38]Y. An, L. Dai, Y. Wu, B. Wu, Y. Zhao, T. Liu, H. Hao, Z. Li, G. Niu, J. Zhang, Z. Quan, and S. Ding, J. Adv. Dielectr. **09**, 1950032 (2019).
[39]N. Blumenschein, T. Paskova, and J. F. Muth, Phys. Status Solidi A **216**, 1900098 (2019).